

**STUDIES ON EFFECTS OF PERIODIC WAKE PASSING UPON A BLADE LEADING EDGE SEPARATION BUBBLE
: TRANSITIONAL BEHAVIORS OF SEPARATED BOUNDARY LAYER**

K. Funazaki¹, K. Yamada¹ and Y. Kato²

¹ **Department of Mechanical Engineering
Iwate University**

3-5, Ueda 4, Morioka 020-8551, Japan

Phone/Fax: +81-19-621-6244, E-mail: funazaki@iwate-u.ac.jp

² **Ishikawajima-Harima Heavy Industries Co.**

ABSTRACT

This paper describes an experimental investigation on aerodynamic interaction between incoming periodic wakes and leading edge separation bubble on a compressor or turbine blade, using a scaled leading edge model that consists of a semi-circular leading edge and two flat-plates. Cylindrical bars of the wake generator produce the periodic wakes in front of the test model. The study aims at deepening the knowledge on how and to what extent the periodic wake passing suppresses the leading edge separation bubble. Special attention is paid to the transitional behaviors of the separated boundary layers. Hot-wire probe measurements are then executed under five different flow conditions to examine effects of Reynolds number, Strouhal number, direction of the bar movement and incidence of the test model against the incoming flow. The measurements reveal that the wake moving over the separation bubble does not directly suppress the separation bubble. Instead, wake-induced turbulence spots and the subsequent calmed regions have dominant impacts on the separation bubble suppression for the all test cases. Numerical simulations are also attempted to grasp an idea how the incoming wakes interact with the separation bubble. A distinct difference is also observed in terms of the bubble suppressing effect by the wakes when the direction of the bar movement is altered.

INTRODUCTION

Recent studies of great numbers have investigated the interaction between periodically incoming wakes and separation bubble on compressor or LP (low-pressure) turbine blades, aiming at the acquisition of detailed information on the behaviors of the wake-affected separation bubble. For example, Halstead et al. (1995a-d) comprehensively reported on ensemble-averaged quasi-wall shear stress on compressor or turbine blades to elucidate the interaction between upstream wakes-the blade boundary layer using test rigs for compressors and turbines. Cumptsy et al. (1995) investigated wake-affected boundary layers accompanied with separation bubble on a compressor cascade. Schulte and Hodson (1994), Kaszeta, Simon and Ashpis (2001), examined wake-separation bubble interaction using linear turbine cascades and moving bars, aiming at the clarification of favorable effects of the wake passing upon the separation in terms of the profile loss reduction.

In contrast to those enriched knowledge concerning the separation bubble on the blade suction surface, there still be less information on the interaction between the incoming wakes and leading edge separation bubble on a compressor or a turbine blade. Except for a pioneering effort done by Paxson and Mayle (1990), few attention was paid to the leading edge flow fields with separation bubble. Recently, Brear et al. (2001) examined flow separation occurring just behind the blade leading edge on the pressure surface of LP turbine cascade subjected to the periodic wakes from the moving bars. Flow visualizations and aerodynamic loss measurements were made in their study, showing that the shear layer was found to be slightly affected by the wake passing or increased free-stream turbulence. Funazaki and Kato (2002), using a simple scaled leading edge model of compressor blade and the moving bar mechanism, executed detailed measurements of the separated boundary layer on the test model affected by the periodic wake passing. Similarly, a simplified flat-plate model experiment was made by Ottavy et al. (2002), followed by Chun and Sung (2002).

The present study is an extended version of the previous study (Funazaki and Kato, 2002) using the almost similar test facility. Focus is on the clarification of the wake-passing effects on transitional behaviors of the separated boundary layers occurring near the leading edge of the test model subjected to various flow conditions. Then one can finally observe the how and to what extent important flow parameters, such as direction of the bar movement, wake-passing Strouhal number, inlet Reynolds number and incident of the model, altered the transitional characteristics of the wake-affected transitional boundary layers. Special attention is paid to the emergence of wake-induced turbulence spots, which was already reported by Funazaki and Kato (2002) with less quantitative discussion, though. Numerical simulation is also made to provide an idea on how the incoming periodic wakes interact with the separation bubble.

NOMENCLATURE

d : bar diameter
 f_{bp} : bar-passing frequency(= U_b / p)
 i : incidence
 N : number of data segments for ensemble-averaging
 p : bar pitch (= 0.3175 m)
 R : radius of the leading edge of the test model

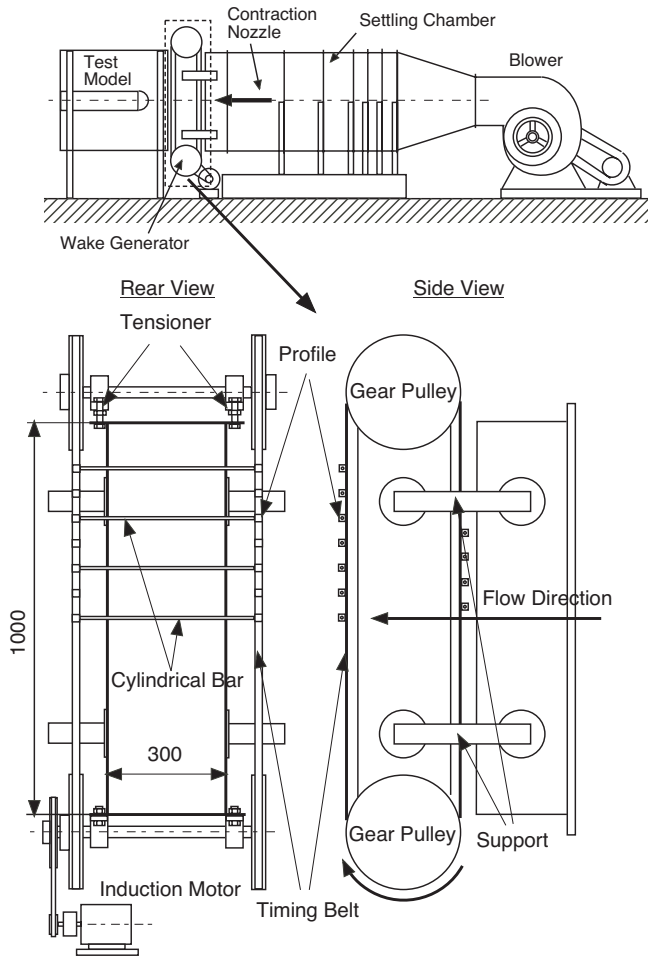


Figure 1 Test apparatus with wake generator

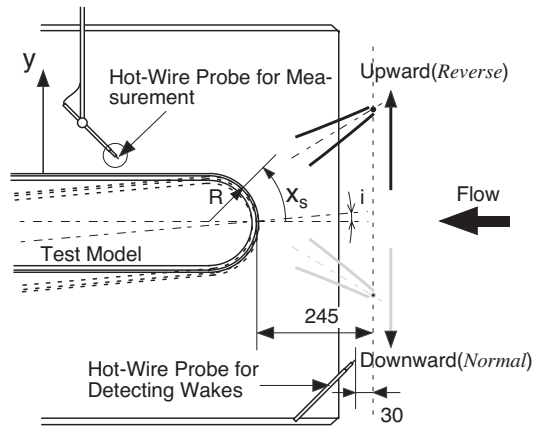


Figure 2 Test model and two hot-wire probes

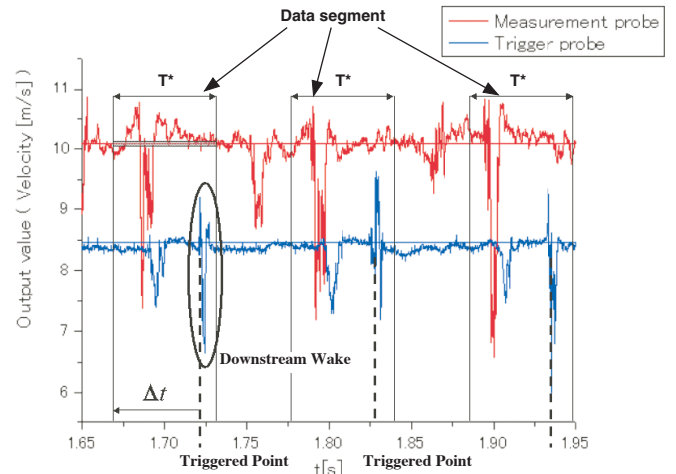


Figure 3 Test model and two hot-wire probes

- Re : Reynolds number ($= U_{in}R/\nu$)
- t : time
- T : bar-passing period ($= p/U_b$)
- T^* : time length of data segment for ensemble averaging
- Tu^* : ensemble-averaged turbulence intensity
- U_b : bar speed
- U_{in} : inlet velocity
- U_{max} : maximum velocity attained near the surface
- U_{ref} : reference velocity measured at $y = 50\text{mm}$
- u_k, u^*, \bar{u} : raw velocity data, ensemble-averaged velocity and time-averaged velocity
- x_s : distance along the surface from the leading edge
- Y : vertical distance from the center line of the test model
- y : vertical distance from the test model surface
- y_{max} : height where the maximum velocity U_{max} appeared
- ν : kinematic viscosity
- δ_1^*, δ_2^* : ensemble-averaged displacement and momentum thickness

EXPERIMENTAL APPARATUS

Test Facility

Test facility used in this study was almost the same as that in the previous study [15]. Figure 1 shows the experimental setup. The wake generator, which was attached to the exit of the contraction nozzle, consisted of two long timing belts, four geared pulleys and stainless-steel bars. The bars of 6mm diameter were tightly fixed to the belts horizontally using connecting profiles glued on both of the belts. The pitch of the profiles was 63.5 mm and the profile number was 50. The induction motor drove the belts at a speed ranging from 4.5 m/s to 7.5 m/s and the direction of the bar movement was revers-

ible. The distance between the upstream and downstream loci of the bars was about 300 mm.

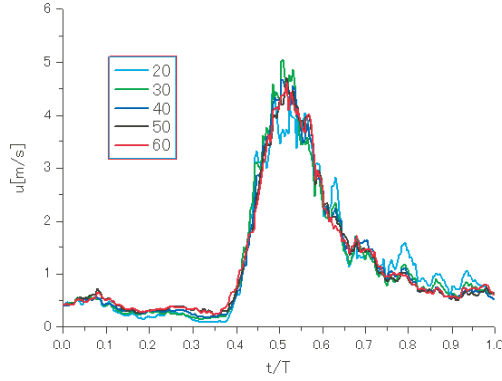
Figure 2 depicts the test model that was in the test duct. The model, with a semi-circular leading edge of 100 mm radius ($= R$) and two flat plates, was 900 mm long and 280 mm wide. Two thin fences were attached to the test model surface near the both side walls of the duct to minimize side-wall contamination. The model was distanced by 245 mm from the downstream locus of the moving bars. A Pitot tube monitored the inlet velocity in front of the test section. The test model could be tilted to change incidence against the inlet flow.

Test Conditions

Table 1 is the test conditions of this study. Test Case 1 was a baseline experiment, where the inlet velocity U_{in} was 10 m/s and the bars moved upwards just in front of the model at a speed of 6 m/s. Reynolds number Re based on the radius of the model leading edge and the inlet velocity was 6.5×10^4 . Test Case 2 aimed at clarification on how differently the wakes generated from the bar moving downwards affected the separation bubble in comparison with the results of Test Case 1. Caution might be necessary in interpretation of the results of Test Case 3 because the wake characteristics might have altered due to the change in relative inlet velocity against the bar. Test Case 4, where the bar speed increased by 25% from the baseline experiment, was for examining the effect of wake-passing frequency or Strouhal number. Reynolds number effects were investigated in Test Case 4, where the bar speed was decreased so as to keep the Strouhal number the same as that of Test Case 1. In Test Case 5 the model was tilted as shown in Figure 3 to change the incidence from 0° to 5° .

Table 1 Test condition

Test Case	Bar Movement	U_{in} [m/s]	U_b [m/s]	$Re \times 10^{-4}$	St	β [deg]
1	Upward	10	6	0.67	0.185	0
2	Downward	10	6	0.67	0.185	0
3	Upward	10	7.5	0.67	0.231	0
4	Upward	7.5	4.5	0.50	0.185	0
5	Upward	10	6	0.67	0.185	5

**Figure 4 Example of convergence histories of the ensemble-averaged velocity**

The measurement region extended from $x_s/R = 0.96$ (55° from the center line) to $x_s/R = 4.57$ in the streamwise direction and from $y/R = 0.3 \times 10^{-2}$ to $y/R = 0.5$ in the vertical direction.

Data Acquisition

Figure 2 clearly indicates that the bars passed across the main flow twice in one revolution of the belts at the different streamwise positions. This inevitably generated two different types of the wakes, ‘upstream wakes’ at the far upstream of the test model and ‘downstream wakes’ near the model. Since this study intended to investigate only the effect of the ‘downstream wakes’, great care was paid to the pitch and the bar count in order to make the measurement time length being undisturbed by the ‘upstream wakes’ as long as possible. Several trials finally found that three bars with the pitch (p) of 317.5 mm on the belts sufficed the above-mentioned requirement.

Two miniature hot-wire probes (Dantec 55P11) appeared in Figure 2, the upper of which was to measure the flow field around the test model, called *measurement probe*. The lower probe, called *trigger probe*, was to detect the arrival of the downstream wakes from the bars. Both probes were connected to CTA unit (Dantec Streamline) that was fully controlled by a PC. Outputs of the hot-wire probes were first compensated to the main flow temperature fluctuation. They were then simultaneously acquired and converted from analog to digital by a built-in A/D converter, finally stored into the PC. Note that for one measurement point the system captured velocity data of 2^{16} word with the sampling frequency of 5kHz, where this relatively low sampling frequency was employed for maximizing the bar wake count in one velocity record.

Ensemble-Average Quantities

Figure 3 shows an example of the velocity signals acquired by the two different probes, indicating the appearance of the two different wakes. Periodic velocity data segments of time length T^* were carefully extracted from the signal of the measurement probe so that the upstream wake was not included in each of the segments. In this case, the downstream wake detected by the trigger probe was used to determine the starting point of each of the data segments.

The sampling frequency was 5kHz and one measurement lasted for about 13 sec ($= 2^{16}/5000$), therefore, the total number of the revolutions of the timing belts during the one measurement was at least 18 even for the slowest belt speed case (Test Case 3). Since one revolution of the belts generated 3 wakes, more than 50 signals of the downstream wakes passing over the boundary layer were avail-

able for each of the realizations. Ensemble-averaged velocity u^* was then calculated from the extracted 50 data segments as follows;

$$u^*(x,y;t) = \frac{1}{N} \sum_{k=1}^N u_k(x,y;t), \quad N = 50. \quad (1)$$

The count of the segments for this ensemble-averaging was rather small in comparison with those commonly used in any other studies, however, as discussed later, $N = 50$ was found to be almost a satisfying count, at least in the present case.

Ensemble-averaged velocity fluctuation $\Delta u_k^*(x,y;t)$ was also evaluated by

$$\Delta u_k^*(x,y;t) = u_k^*(x,y;t) - \bar{u}(x,y), \quad (2)$$

where $\bar{u}(x,y)$ was time-averaged velocity calculated by

$$\bar{u}(x,y) = \frac{1}{T} \int_{t_0}^{t_0+T} u^*(x,y;t) dt. \quad (3)$$

Ensemble-averaged turbulence intensity was also defined as,

$$Tu^*(x,y;t) = \sqrt{\frac{1}{N-1} \sum_{k=1}^N \Delta u_k^{*2}} / U_{ref}, \quad (4)$$

where U_{ref} was reference velocity, and in this case time-averaged velocity obtained at the upper limit of the measurement region $y/R = 0.5$ was adopted as the reference velocity.

The following expressions were employed to calculate boundary layer integral parameters using the ensemble-averaged velocity;

$$\delta_1^*(x;t) = \int_0^{y_{max}(x;t)} \left(1 - \frac{u^*(x;t)}{U_{max}(x;t)} \right) dy, \quad (5)$$

$$\delta_2^*(x;t) = \int_0^{y_{max}(x;t)} \frac{u^*(x;t)}{U_{max}(x;t)} \left(1 - \frac{u^*(x;t)}{U_{max}(x;t)} \right) dy, \quad (6)$$

where δ_1^* and δ_2^* were ensemble-averaged displacement thickness and momentum thickness, respectively. Note that $y_{max}(x,t)$ was the location where the velocity reached the maximum $U_{max}(x,t)$ in the vicinity of the test model surface and regarded as the boundary layer thickness in this study.

Uncertainty Analysis

Since the calibration curve of a 4-th order polynomial matched the velocity data measured with a pneumatic probe quite well, a major contributor to the uncertainty in the velocity data acquired by the hot-wire probe was the error in the pneumatic probe measurement. This error, mainly depending on the accuracy of the pressure transducer used, was estimated to be about ± 0.6 [m/s].

Besides, the convergence rate of the ensemble-averaging surely had a serious impact on the uncertainty of the resultant velocity. Figure 4 shows an example of the convergence histories of the ensemble averaging with the increase of N , using the experimental raw data at $x_s/R = 1.695$ and $y/R = 0.05$. It seems that the ensemble-averaged velocity calculated from more than 50 velocity segments almost got converged, with the average residual less than 0.05 [m/s].

Single hot-wire probes cannot detect reversed flow without any manipulations, so that the present measurements inevitably suffered from the under- or overestimations of the boundary layer integral parameters given by Eqs. (5) and (6). Detailed investigations revealed that in the no wake case, which was the worst case, the displacement thickness was underestimated by 7% and the momentum thicknesses were overestimated by 50%, respectively, at the position where the reversed flow became active most.

NUMERICAL SCHEME

Flow Solver and Computing System

Unsteady three-dimensional flow simulations were performed by solving the compressible Navier-Stokes equations using an unfactored implicit upwind relaxation scheme with inner iterations (Furukawa et al. (1992)). The numerical method used is outlined in the following. The three-dimensional Reynolds-averaged Navier-Stokes equations were discretized in space using a cell-centered finite volume formulation and in time using the Euler implicit method. The inviscid fluxes were evaluated by a high-resolution upwind scheme based on a TVD formulation (Furukawa et al. (1991)), where a Roe's approximate Riemann solver of Chakravarthy (1986) and a third-order accurate MUSCL approach of Anderson et al. (1986) with the Van Albada limiter were implemented. The viscous fluxes were evaluated in a central-difference manner. The $k-\omega$ turbulence model (Wilcox(1988)) was employed to estimate the eddy viscosity. Simultaneous equations linearized in time were solved by a point Gauss-Seidel relaxation method using no approximate factorization. To obtain a time-accurate solution, inner iterations, so-called Newton iterations were introduced at each time step. The scheme was kept second-order accurate in time by applying the three-point-backward difference approximation to the temporal derivative. For the unsteady flow simulations presented in this paper, nine inner iterations were performed at each time step, and a nondimensional time step size normalized by the radius of the model and the inlet sound speed was set to 0.2.

The computing system used was a PC-cluster with 8 nodes, each of which contained one Intel Xeon processor of 2.4GHz speed and 6MB main memory. Gigabit and megabit network system was constructed in the PC-cluster, where the gigabit system exchange the numerical data and the megabit system was for network operation such as NFS.

Grid System and Boundary Conditions

The code was parallelized using MPI (Message Passing Interface), and a five-block grid system shown in Figure 5 was adopted in this simulation. Information on grid points in each block is listed in Figure 5. The spanwise length of the system was relatively short because the flow field concerned was almost two-dimensional. To emulate the experiment, equally spaced wake profiles that were experimentally determined were specified on the inlet plane. These wake profiles slid along the inlet plane at the bar speed U_b . Other boundary conditions such as inlet velocity or inlet Reynolds number were the same as that of the experiments.

RESULTS

Steady-State Flow Measurements

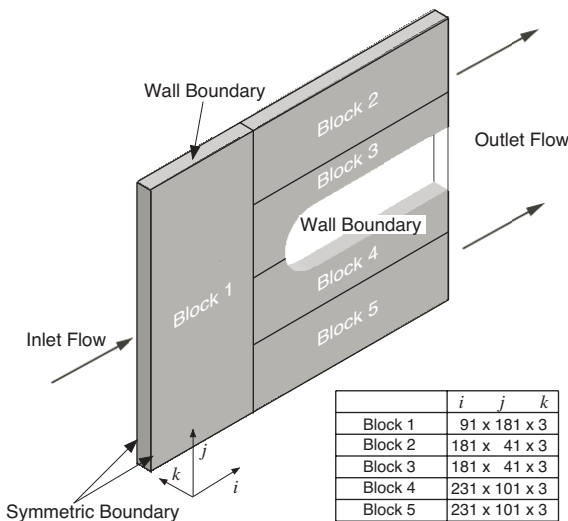


Figure 5 Multi-block grid system used in the simulation

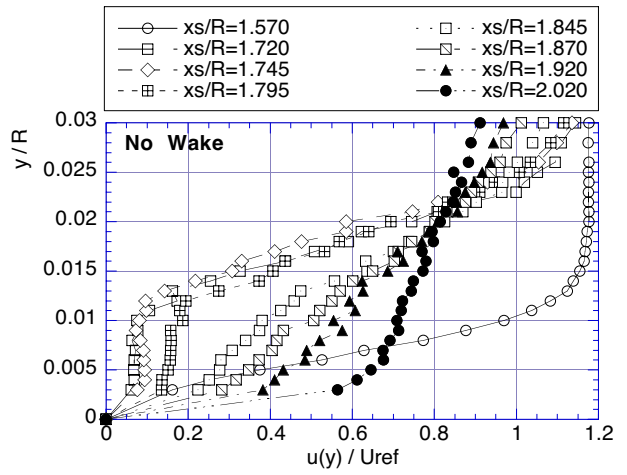


Figure 6 Velocity profiles of the separated boundary layer for no wake condition

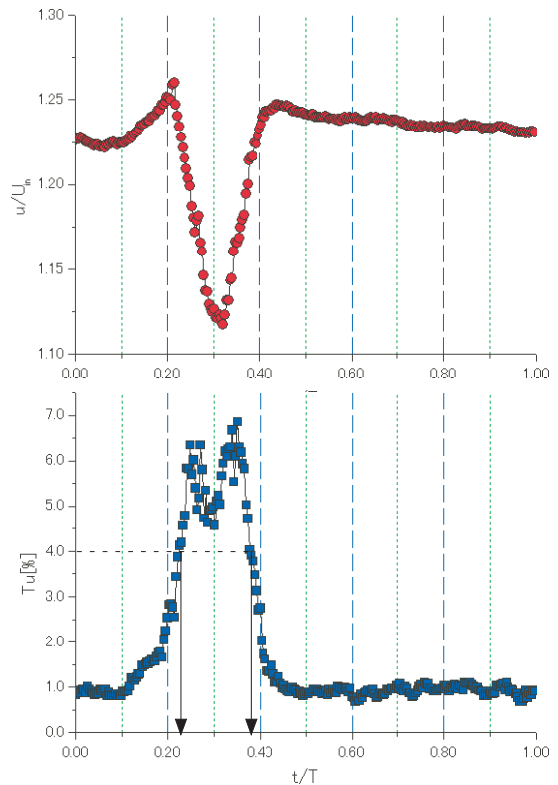


Figure 7 Velocity (upper) and turbulence intensity (lower) profiles in the wake generated by the moving bar of 6mm diameter. (location : $x/R=1.308$, $y/R=0.5$)

Figure 6 displays velocity profiles of the separated boundary layer measured at several streamwise stations without the bar wake influence. The velocity at any streamwise position was normalized by its reference velocity U_{ref} . The separation occurred almost at the junction of semi-circular leading edge and the flat plate, because of the difference in curvature. The thickness of the separation bubble was found to be about 2.0mm (0.02 when normalized by R). Comparing these profiles with Horton's mean reattachment profile (Horton, 1968), it was found that the reattachment point located around $x_s/R=1.87$.

Wake Profile

Figure 7 shows ensemble-averaged velocity and turbulence intensity of the moving-bar wake of Test Case 1. They were measured by the hot-wire probe located near the leading edge of the test model

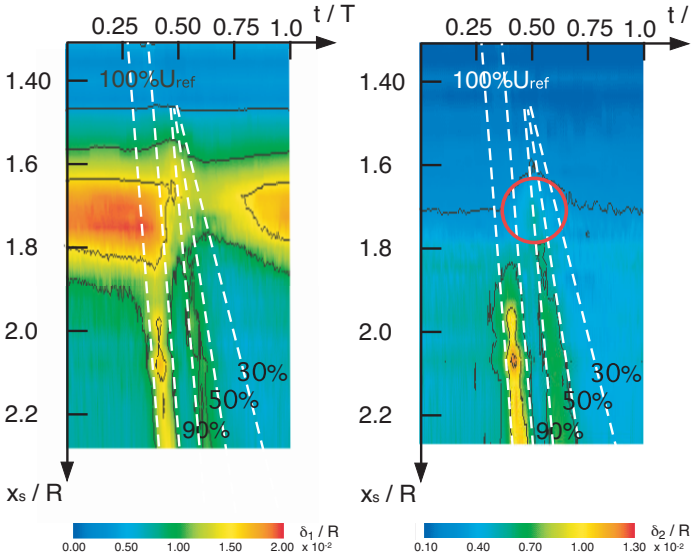


Figure 8 Ensemble-averaged displacement and momentum thicknesses on x_s - time planes for Test case 1 (left : Displacement thickness / right : Momentum Thickness)

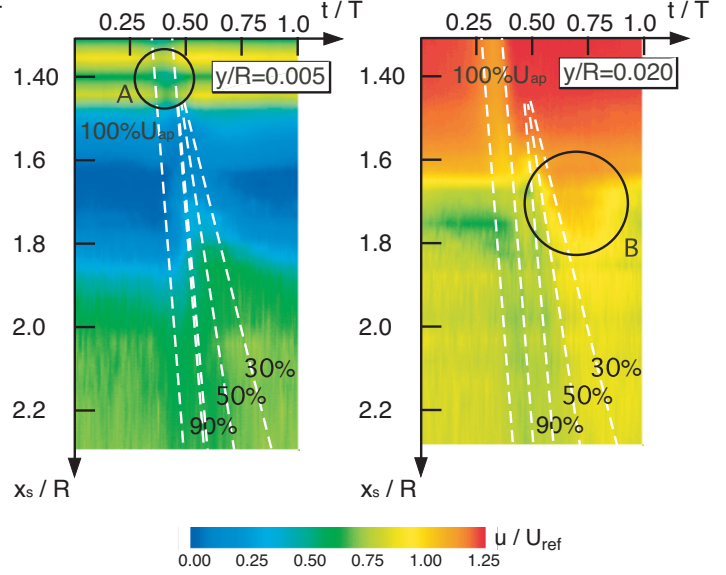


Figure 10 Ensemble-averaged velocity on x_s - time planes for Test case 1 (left : $y/R = 0.005$ / right : $y/R = 0.020$)

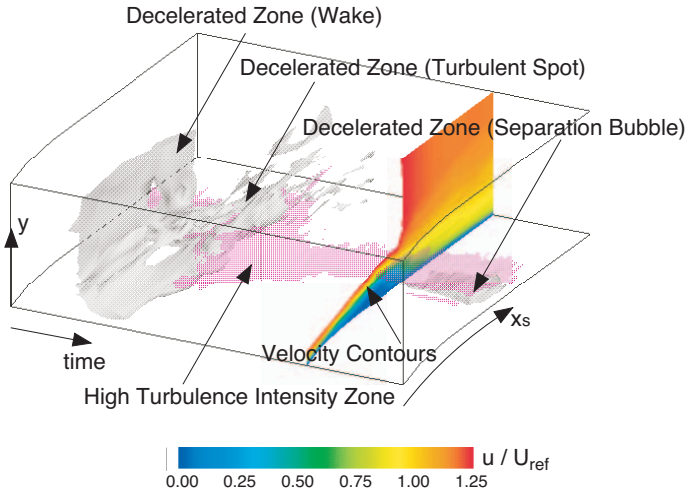


Figure 9 Composite 3D representation showing velocity fluctuation, turbulence intensity and velocity profile for Test case 1

($x_s/R = 1.308$ and $y/R = 0.5$) during one wake passing period. The data shown here was normalized by the inlet velocity U_{in} . Despite a flow acceleration near the leading edge, the velocity deficit of the wake retained about $0.2 U_{in}$ and the maximum wake turbulence was about 7%. Note that two peaks in the turbulence intensity due to the shear layer of the wake were clearly observed. It follows from this figure that the wake with more than 4% turbulence intensity, which can be regarded as an effective turbulence intensity according to the suggestion of Funazaki et al. (1997), lasted for about 15% of the bar passing period.

Emergence of Turbulence Spots and Calmed Region

Discussion using boundary layer parameters Figure 8 shows contours of the ensemble-averaged displacement and momentum thicknesses on the x_s -time plane for Test Case 1 (the bar moving upwards). Also shown in this figure are five lines on each of the contours, which represent traces of the fluid particles moving at 100%, 90%, 50% and 30% speed of U_{ref} , streamwisely averaged velocity of U_{ref} over the measurement region. In Figure 8, the wide zone of

large displacement thickness appeared from $x_s/R = 1.6$ to $x_s/R = 1.8$, which was caused by the separation bubble.

Before going into detail of the wake interaction with the separation bubble, a brief comment seems necessary on how the positions of those lines were determined. Because of its low velocity and consequently large value of y_{max} , the incoming wake tended to leave its footprint in terms of a strip of relatively large displacement thickness. Taking advantage of this tendency, the wake path on the contour of the displacement thickness was easily spotted as shown in the left contours of Figure 8. The positions of the 100% speed traces were accordingly determined so that they fitted the strip of large displacement thickness. There appeared a triangle zone of large value on the displacement thickness contours. Since this zone could be regarded as a consequence of wake-induced turbulence spots growing towards the downstream, particle traces of 90% and 50% speed were chosen to sketch out the zone, where the starting points of each of the traces were placed on the same position. A trace of 30% speed, which may represent the rear end of calmed region [1], also started from the same point as the 90% and 50% traces. The same traces were used in the momentum thickness contours without any modifications. It turned out that the procedure to determine the positions of the traces worked quite well in Test Case 1, and as will be shown in the following, the same approach was actually found to be valid in other test cases, except for Test Case 2.

From the above discussions, it can be concluded that the triangle-shaped zone of large displacement thickness identified after the wake passage was the consequence of wake-induced turbulence spots. Besides, the momentum thickness data elucidated an area marked by the circle. This area, which had relatively larger momentum thickness inside, almost laid itself underneath the path enclosed by 90% and 50% speed traces. Since increase in momentum thickness usually means the progress of boundary layer transition, the appearance of this area also supports the conclusion here that the incoming wake induced turbulent spots that strongly affected the separation bubble. The important point here is that the spots in this case abruptly emerged almost at or rather upstream of the separation point. This was probably because of the adverse pressure gradient observed by Funazaki et al. (2000) or the change in curvature as a catalyst of the transition, although much remains to be studied in the future. As discussed in the following, onset points of the turbulent spots, which were determined by the curve-fitting approach, exhibited a slight dependency to the flow conditions such as Reynolds number or Strouhal number.

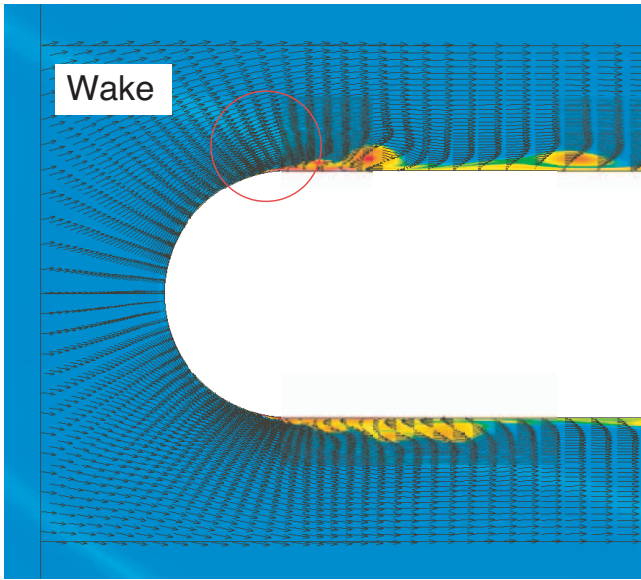


Figure 11 Computed result of wake-leading edge interaction

Discussion using velocity fluctuation and turbulence intensity Figure 9 shows a composite representation of velocity fluctuation, turbulence intensity and velocity profile in x_s, y and time domain for Test Case 1. This figure clearly demonstrates the existence of the incoming wake and the appearance of the induced turbulence spots behind the wake in terms of the decelerated zone, where the deceleration was measured from the local averaged velocity (see Eq. (2)). High turbulence intensity zone, which contained more than 14% local turbulence intensity and was pink-colored in this figure, started to shrink after the passage of those decelerated zone. Since the high turbulence intensity originated mostly from unstable shear layer of the separation bubble, this shrinkage indicated that the wake passage surely suppressed the separation bubble for relatively long period.

Effects of the Bar-Moving Direction and Strouhal Number

Test Case 1 (bar moving upwards) In Test Case 1, baseline case, the wide zone having large displacement thickness almost disappeared while the incoming wake swept over the test model, then recovered afterwards. This indicates that the leading separation bubble experienced temporal suppression because of the passage of the incoming wake. Important features to be mentioned were found in Figure 8. The observation shows that the separation bubble with large displacement thickness remained almost unaffected even just beneath the wake path. It seems that the wake passage itself did not make an explicit contribution to the suppression of the separation bubble in this case. In contrast, the reduction of the displacement thickness indicates that the wake-induced turbulence spots and the following calmed region surely suppressed the separation bubble. A similar conclusion can be drawn from the observations of the ensemble-averaged velocity in Figure 10, where the low speed zone associated with the separation bubble became small when the turbulent spots, then the calmed region passed over the separation bubble.

The turbulent spots, whose origin was identifiable from the intersection of the traces, slightly lagged behind the wake passage in this case. The footprints of the wake passage could be recognized on the near-wall plane ($y/R = 0.005$) as well as on the plane with its height from the wall almost same as that of the separation bubble ($y/R = 0.020$). On the plane of $y/R = 0.005$ in Figure 10, the 100% speed traces could be shifted in the right direction from the original position of Figure 8 by some distance so that the traces agreed with the wake passage footprint at the location denoted by the circle A. Since this shifting resulted in the attachment of the 100% traces to

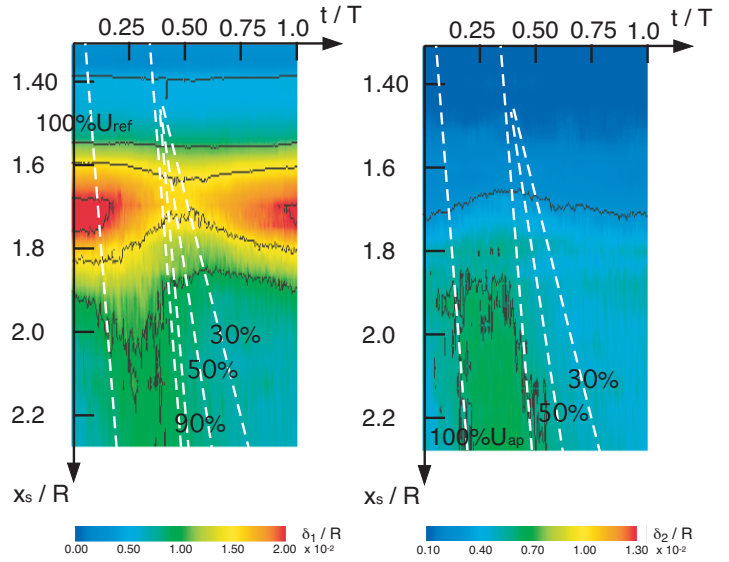


Figure 12 Ensemble-averaged displacement and momentum thicknesses on x_s - time planes for Test case 2 (left : Displacement thickness / right : Momentum Thickness)

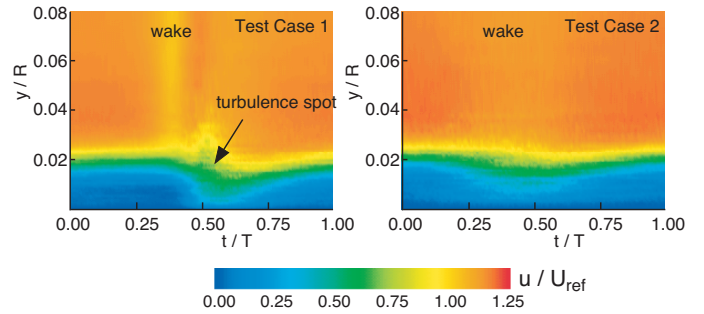


Figure 13 Bar wakes interacting with the separation bubble on y - time planes of ensemble-averaged velocity measured at $x_s/R = 1.745$ (left : Test Case 1 / right : Test Case 2)

the other traces, it can be stated that the turbulence spots actually emerged just after the wake passage near the surface. In other words, the upstream wake was mainly responsible for the generation of the turbulent spots. The shifted distance of the traces corresponded to about 7% of the wake passing period, meaning that the wake suffered from large deformation due to the blockage effect of the test model and/or lagged behind the free-stream within the boundary layer.

Circle B in Figure 10 shows that the separation bubble did not fully recover from the wake of the upstream wake passing even after the passage of the turbulent spots and the calmed region. One possible reasoning on this phenomenon is “negative-jet effect” of the upstream wake interacting with the leading edge of the test model.

Figure 11 shows a snapshot of the numerical simulations showing the sequential interaction of the wake with separation bubbles on the both sides of the test model. The predicted separation bubble exhibited considerable unsteady feature such as vortex shedding in a periodic manner. Although the code lacked ability to predict the transitional behavior of the shear layer of the separation bubble, the size of the bubble seemed to be reasonably predicted. The shed vortices moving downstream were considerably large in comparison with the size of the test model, which could not be verified through the present experiment because the shedding of the vortices was not necessarily synchronized with the bar passing and the ensemble-averaging could not properly capture such non-synchronized flow

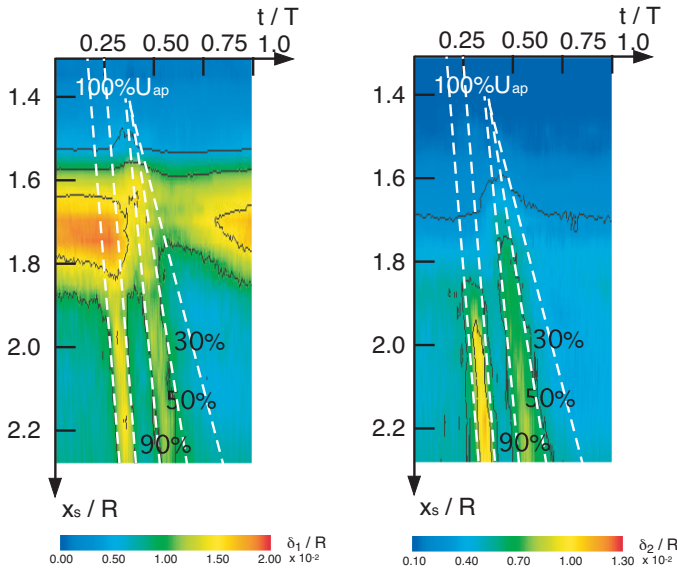


Figure 14 Ensemble-averaged displacement and momentum thicknesses on x_s - time planes for Test case 3 (left : Displacement thickness / right : Momentum Thickness)

event.

Figure 11 indicates that the wake deformed around the leading edge, interacting with the separation bubble. At a first glance, it does not seem that the wake passage had a drastic impact on the separation bubble, which matches the experimental observation shown in Figure 9. However, the code was not able to predict the emergence of turbulence spot. This means many subjects are left to be tackled in order to improve the ability of the code.

Test Case 2 (bar moving downwards) Figure 12 depicts contours of the ensemble-averaged displacement and momentum thicknesses on the x_s -time plane for Test Case 2 (the bar moving downwards). Clearly, the wake duration in Test Case 2 was much longer than that of Test Case 1. The separation bubble was gradually shrunk but not fully extinguished while the wake passed over it, which was in contrast to Test Case 1. Rather surprisingly, wake-induced turbulence spots and calmed region were not clearly seen in this figure, although the separation bubble was still suppressed even after the wake passage. The appearance of the larger wake duration in the *normal* moving case was already reported by Funazaki et al. (1997), which was also due to “negative-jet effect”. Figure 13 shows the ensemble-averaged velocities on the y -time planes for Test Case 1 (left) and Test Case 2 (right), again emphasizing the difference between the two cases in terms of bar-wake interaction with the separation bubble. The data in this figure was acquired at $x_s/R = 1.745$ where the separation bubble reached its maximum height in no wake case as shown in Figure 5. The left contours in Figure 13 clearly depict that turbulent spots appeared behind the wake, penetrating the free-stream. Underneath the turbulent spots, the separation bubble, which was expressed by very low speed zone, was temporarily diminished. On the contrary, the wake in Test Case 2 was rather vague and did not seem to be accompanied by any turbulence spots. Furthermore, the separation bubble in this case was not completely extinguished, while it experienced the wake passage and its influence for longer time than in Test Case 1. At this moment the reason for this distinct difference has not been clarified yet.

Test Case 3 (higher Strouhal number) Figure 14 is the results of Test Case 3; higher Strouhal number case. Since the Strouhal number increased only by 25% of the original value, overall views of the displacement and momentum thickness contours quite resembled

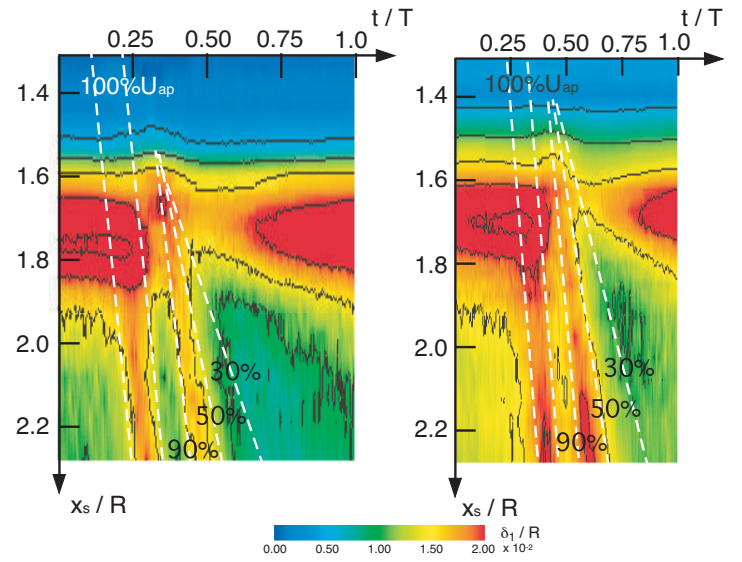


Figure 15 Ensemble-averaged displacement and momentum thicknesses on x_s - time planes for Test case 3 (left : Test Case 4 / right : Test Case 5)

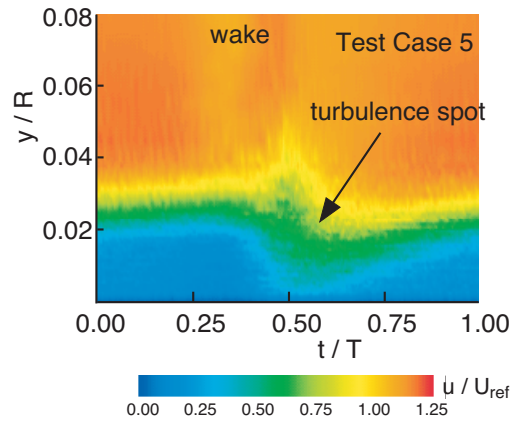


Figure 16 Bar wakes interacting with the separation bubble on y - time planes of ensemble-averaged velocity measured at $x_s/R = 1.745$ (Test Case 5)

those of Test Case 1. However, the onset of the wake-induced turbulence spots, which could be regarded as virtual origin of the spots, took place a little earlier than in Test Case 1, probably because of enhanced wake turbulence.

Effects of the Mean Flow Conditions

Figure 15 shows two contours of the wake-affected displacement thickness on x_s -time diagrams obtained for Test Case 4 and Test Case 5. Since the Reynolds number was reduced by 25% in Test Case 4 or the incidence was increased from 0 deg to 5 deg, the separation bubble for each of the test cases was larger than Test case 1, which could be confirmed by looking at the extent of the high displacement thickness zone as well as at the peak value within the zone. Wake-induced turbulence spots clearly appeared, slowly being lagged from the wake in both test cases. The onset of the turbulent spots in Test Case 4 (left of Figure 15) was found around $x_s/R = 1.6$, while $x_s/R = 1.5$ for Test case 1. This delay could be attributed to the effect of the reduced Reynolds number. On the other hand, the onset of the wake-induced turbulence spots in Test case 5 started earlier than in Test case 1. This was probably because in effect the surface length from the aerodynamic stagnation point to a point concerned was elongated by about 0.09 in x_s/R . Figure 16, ensemble-averaged velocity measured at $x_s/R = 1.745$, indicates

that wake-induced turbulent spots appeared behind the wake, abruptly diminishing the separation bubble of very low speed zone. Thereafter, the separation bubble started to recover in a gradual manner.

CONCLUSIONS

This study dealt with hot-wire probe measurements of separated boundary layer around the leading edge of the blunt test model which was subjected to periodic wake passing. The focus of this study was on the effects of the direction of the wake-generating bar movement, wake-passing Strouhal number and the mean flow conditions such as Reynolds number. The findings in this study can be summarized as follows.

- (1) When the wake-generating bar moved upwards, the emergence of wake-induced turbulence spot, followed by the resultant calmed region, were identified behind the downstream wake in the contours of the time-resolved displacement and momentum thicknesses on the distance-time planes or the ensemble-averaged velocity.
- (2) The turbulent spots emerged almost at or rather upstream of the separation point. This rather early emergence of the turbulent spots could be reasoned by the effect of adverse pressure gradient or the change in curvature as a catalyst of the transition, although much remains to be studied in more detail. The onset of the turbulent spots onset slightly depended on the flow conditions such as Reynolds number or Strouhal number.
- (3) The wake generated from the bar moving upwards did not make an explicit contribution to the suppression of the separation bubble. This was confirmed by the numerical simulation. On the contrary, the wake-induced turbulence spots and the following calmed region suppressed the separation bubble. The wake-affected separation bubble did not show quick recovery to the state of no wake condition after the wake passage. One possible explanation on this phenomenon was "negative-jet effect" of the upstream wake interacting with the leading edge of the model.
- (4) Wake-induced turbulence spots and calmed region were not clearly observed in the case when the wake-generating bar moved downwards.

ACKNOWLEDGMENTS

The part of this work was conducted under the financial support from the Ministry of Education and Science as Grants-in-Aid for Scientific Research. The authors are indebted to invaluable supports from Mr. F. Saito of Iwate University.

REFERENCES

- Anderson, W. K., Thomas, J. L., and van Leer, B., 1986, "Comparison of Finite Volume Flux Vector Splittings for the Euler Equations, AIAA Journal, Vol. 24, No.9, pp. 1453-1460.
- Brear, M.J., Hodson, H.P. and Harvey, N.W., 2001, "Pressure Surface Separations in Low Pressure Turbines: Part 1 of 2 - Midspan Behaviour," ASME Paper 2001-GT-0437.
- Chakravarthy, S. R., 1984, "Relaxation Method for Unfactored Implicit Upwind Schemes," AIAA Paper No. 84-0165.
- Chun, S. and Sung, J., 2002, "Influence of Unsteady Wake on a Turbulent Separation Bubble," Experiments in Fluids, Vol. 32, pp.269-279.
- Cumptsy, N.A., Dong, Y., and Li, Y.S., 1995, "Compressor Blade Boundary Layers in the Presence of Wakes," ASME Paper 95-GT-443.
- Halstead, D.E., Wisler, D.C., Okiishi, T.H., Walker, G.J., Hodson, H.P. and Shin, H.-W., 1995a, "Boundary layer Development in Axial Compressors and Turbines, Part 1 of 4: Composite Picture," ASME Trans., Journal of Turbomachinery, Vol. 119, pp. 114-127.
- Funazaki, K., Harada, Y., Takahashi, E., 2000, "Control of Separation Bubble on a Blade Leading Edge by a Stationary bar Wake," ASME Paper 2000-GT-267.
- Funazaki, K. and Kato, Y., 2002, "Studies on a Blade Leading Edge Separation Bubble Affected by Periodic Wakes: Its Transitional

Behavior and Boundary Layer Loss Reduction," ASME Paper GT-2002-30221.

Funazaki, K., Kitazawa, T., Koizumi, K. and Tanuma, T., 1997, "Studies on Wake-Disturbed Boundary layers under the Influences of Favorable Pressure Gradient and Free-Stream Turbulence-Part I: Experimental Setup and Discussions on Transition Model," ASME Paper 97-GT-52.

Furukawa, M., Nakano, T., and Inoue, M., 1992, "Unsteady Navier-Stokes Simulation of Transonic Cascade Flow Using an Unfactored Implicit Upwind Relaxation Scheme With Inner Iterations," ASME Trans., Journal of Turbomachinery, Vol. 114, No.3, pp. 599-606.

Furukawa, M., Yamasaki, M., and Inoue, M., 1991, "A Zonal Approach for Navier-Stokes Computations of Compressible Cascade Flow Fields Using a TVD Finite Volume Method," ASME Trans., Journal of Turbomachinery, Vol. 113, No.4, pp. 573-582.

Halstead, D.E., Wisler, D.C., Okiishi, T.H., Walker, G.J., Hodson, H.P. and Shin, H.-W., 1995b, "Boundary layer Development in Axial Compressors and Turbines, Part 2 of 4: Compressors," ASME Trans., Journal of Turbomachinery, Vol. 119, pp. 426-444.

Halstead, D.E., Wisler, D.C., Okiishi, T.H., Walker, G.J., Hodson, H.P. and Shin, H.-W., 1995c, "Boundary layer Development in Axial Compressors and Turbines, Part 3 of 4: Low Pressure Turbines," ASME Trans., Journal of Turbomachinery, Vol. 119, pp. 225-237.

Halstead, D.E., Wisler, D.C., Okiishi, T.H., Walker, G.J., Hodson, H.P. and Shin, H.-W., 1995d, "Boundary layer Development in Axial Compressors and Turbines, Part 4 of 4: Computations and Analyses," ASME Trans., Journal of Turbomachinery, Vol. 119, pp. 225-237.

Horton, H.P., 1968, "A Semi-Empirical Theory for the Growth and Bursting of Laminar Separation Bubbles," Aeronautical Research Council, CP-1073.

Kaszeta, R.W., Simon, T.W. and Ashpis, D.E., 2001, "Experimental Investigation of Transition to Turbulence as Affected by Passing Wakes," ASME Paper 2001-GT-0195.

Ottavy, X., Vilmin, S., Opoka, M., Hodson, H. and Gallimore, S., 2002, "The Effects of Wake-Passing Unsteadiness over a Highly Loaded Compressor-Like Flat Plate," ASME Paper GT-2002-30354.

Paxson, D.E. and Mayle, R.E., 1990, "Laminar Boundary Layer Interaction with an Unsteady Passing Wake," ASME Paper 90-GT-120.

Schulte, V. and Hodson, H.P., 1994, "Wake-Separation Bubble Interaction in Low Pressure Turbines," AIAA Paper AIAA-94-2931.

Van Treuren, K. W., Simon, T., von Koller, M., Byerley, A.R., Baughn, J.W. and Rivir, R., 2002, "Measurements in a Turbine Cascade Flow under Ultra Low Reynolds Number Conditions," ASME Trans., J. Turbomachinery, 124, pp. 100-106.

Wilcox, D. C., 1988, "Reassessment of the Scale-Determining Equation of Advanced Turbulence Models," AIAA Journal, Vol. 26, No. 11, pp. 1299-1310.